

Zweitveröffentlichung/ Secondary Publication



Staats- und
Universitätsbibliothek
Bremen

<https://media.suub.uni-bremen.de>

André F. Müller, Ralf B. Bergmann, Claas Falldorf

High resolution lensless microscopy based on Fresnel propagation

Journal Article as: published version (Version of Record)

DOI of this document* (secondary publication): <https://doi.org/10.26092/elib/3125>

Publication date of this document: 25/07/2024

* for better findability or for reliable citation

Recommended Citation (primary publication/Version of Record) incl. DOI:

André F. Müller, Ralf B. Bergmann, Claas Falldorf: High resolution lensless microscopy based on Fresnel propagation
Optical Engineering, Vol. 63, Issue 11, 111805 (July 2024)
<https://doi.org/10.1117/1.OE.63.11.111805>

Please note that the version of this document may differ from the final published version (Version of Record/primary publication) in terms of copy-editing, pagination, publication date and DOI. Please cite the version that you actually used. Before citing, you are also advised to check the publisher's website for any subsequent corrections or retractions (see also <https://retractionwatch.com/>).

This document is made available with all rights reserved.

Take down policy

If you believe that this document or any material on this site infringes copyright, please contact publizieren@suub.uni-bremen.de with full details and we will remove access to the material.

High resolution lensless microscopy based on Fresnel propagation

André F. Müller¹, Ralf B. Bergmann^{1,2} and Claas Falldorf¹

¹BIAS - Bremer Institut für angewandte Strahltechnik, Bremen, Germany

²Universität Bremen, Fachbereich 01: Physik und Electrotechnik, MAPEX Center for Materials and Processes, Bremen, Germany

ABSTRACT. Digital holography allows for the recording and reconstruction of three-dimensional images using interference and diffraction principles. The propagation of light from the hologram plane to the reconstruction plane is a crucial step, often achieved through Fresnel propagation, a method that inherently transforms the reconstructed pixel pitch to provide diffraction-limited imaging. However, the accuracy of this method is limited by the Fresnel approximation, especially in applications such as digital holographic microscopy. We present a simple method that significantly improves the accuracy of the Fresnel approximation by incorporating higher orders of the binomial approximation. We validate the effectiveness of our approach through high numerical aperture simulations and experimental results, demonstrating superior sub-micron resolution and reduced distortions compared with standard Fresnel propagation.

© 2024 Society of Photo-Optical Instrumentation Engineers (SPIE) [DOI: [10.1117/1.OE.63.11.111805](https://doi.org/10.1117/1.OE.63.11.111805)]

Keywords: lensless imaging; lensless microscopy; digital holography; microscopy; wave field propagation

Paper 20240306SS received Mar. 28, 2024; revised Jun. 19, 2024; accepted Jun. 24, 2024; published Jul. 12, 2024.

1 Introduction

Digital holography is a powerful technique that enables the recording and reconstruction of three-dimensional (3D) images. By leveraging principles of interference and diffraction, digital holography enables the recording and storage of both amplitude and phase information of light waves scattered from objects.^{1,2} This approach not only eliminates the need for complex optical components but also offers unique advantages such as enhanced depth of focus, volumetric imaging, and precise determination of optical paths at the nanometer scale.³ Digital holography finds applications across various fields, such as metrology,⁴⁻⁶ biomedical imaging,^{7,8} or holographic displays.⁹⁻¹² Another notable application is lensless holographic microscopy.^{13,14}

Due to advancements in image sensor technology as well as improvements in computing power and reconstruction algorithms, lensless holographic microscopy has emerged as a compelling alternative to lens-based microscopy.¹⁵ Because it forgoes expensive and heavy microscope objectives, lensless microscopy methods may provide a cost-effective and field-portable means to achieve depth-resolved 3D imaging.^{16,17} However, it is widely believed that the spatial resolution of lensless holographic microscopes is limited by the pixel pitch of the camera sensor.^{18,19} Several reconstruction algorithms containing an adjustable magnification along varying pixel grids have been proposed,²⁰ scaling the reconstruction either to image objects larger than the sensor²¹ or magnifying the reconstruction of objects containing features smaller than the

*Address all correspondence to André F. Müller, amueller@bias.de

sensors pixel pitch. Their applicability for lensless microscopy is, however, often limited by approximations, implicitly assuming small numerical apertures.²²

This limitation is generally overcome through laborious pixel super-resolution techniques^{23,24} to synthesize a larger and higher resolved hologram.²⁵ This is generally done by recording multiple holograms and scanning either by shifting the camera sensor,^{26,27} object,^{28,29} or illumination^{30,31} or by placing a diffraction grating between sample and camera.^{32,33} However, these techniques generally impose strict limitations on the measurement of transient processes as multiple measurements must be taken sequentially.

One other potential solution for reconstructing holograms measured along a large sized sensor grid onto a higher resolved grid in the object plane is the Fresnel propagation,^{34,35} a method for calculating the propagation of light in homogeneous media that has been widely employed in digital holography due to its simplicity and efficiency. It only requires a single Fourier transform to calculate the wavefront at a desired distance from the hologram plane. Yet, the main advantage of Fresnel propagation, compared with other methods such as plane wave decomposition, is that it accommodates different sampling schemes for the hologram plane and the reconstruction plane.² In discrete implementation in particular, this ensures transformation from a sampling lattice with pixel pitch Δx in the hologram plane to a sampling lattice with pixel pitch

$$\Delta u = \lambda z/L, \quad (1)$$

in the object plane, where λ , z , and L are the wavelength, propagation distance, and size of the hologram plane, respectively. The scaling by the factor of $\lambda z/L \approx \lambda/2$ NA corresponds conveniently to the diffraction limited optical resolution $\delta = \lambda/2$ NA achievable with the propagation process, which therefore prevents the calculation of unnecessary data (oversampling). This means a substantial benefit, especially in applications such as digital holographic microscopy, in which the aimed optical resolution in the object plane is typically in the single micrometer range or even below while the pixel pitch of the camera can be one order of magnitude larger.

However, despite its usefulness, Fresnel propagation is subject to certain limitations. A major drawback is its reliance on the Fresnel approximation,³⁶ which assumes small numerical apertures. This limitation restricts its applicability, particularly in microscopy scenarios, to $\text{NA} < 0.1$. Here, we present a simple solution to overcome this problem and improve the accuracy of the Fresnel approximation. The idea is to incorporate higher orders of the binomial approximation of the square root. We show in both simulations and experiments that this improves the approximation substantially, so that the Fresnel approximation can be applied even in situations in which $\text{NA} \approx 0.5$ holds. Furthermore, the method does not require any additional computational effort and can be easily implemented into already existing propagation algorithms and routines.

2 Methods

2.1 Locally Improved Fresnel Approximation

The starting point of our discussion is the Rayleigh-Sommerfeld diffraction equation. Within the scalar diffraction theory, it provides an exact description of light propagation from an object plane u, v into a hologram plane x, y :³⁷

$$U_H(x, y) = -\frac{1}{2\pi} \int U_O(u, v) \cdot \frac{\exp(ikr)}{r} \cdot \frac{z}{r} \cdot \left(ik - \frac{1}{r} \right) dudv. \quad (2)$$

Here, $U_H(u, v)$ and $U_O(x, y)$ are the complex amplitudes of the wave field across the hologram plane and the object plane, respectively; z is the propagation distance; and $r = \sqrt{(x-u)^2 + (y-v)^2 + z^2}$ is the distance between two points in the hologram plane and the object plane. The Fresnel approximations assume $r \approx z$ outside the exponentials, $ik - 1/r \approx ik$ and a first order binomial approximation of r within the exponentials

$$r \approx z + \frac{1}{2z} [(x-u)^2 + (y-v)^2]. \quad (3)$$

With the Fresnel approximations in place, it is straightforward to reformulate Eq. (2) into a single Fourier transform to obtain the Fresnel propagation equation:³⁶

$$U_H(x, y) = -\frac{i}{\lambda z} S_1(x, y) \cdot \mathcal{F}\{U_O(u, v) \cdot S_2(u, v)\} \left(\frac{x}{\lambda z}, \frac{y}{\lambda z} \right), \quad (4)$$

with the Fourier transform operator \mathcal{F} and two parabolic phase functions

$$S_1(x, y) = \exp \left[\frac{ik(x^2 + y^2)}{2z} + ikz \right] \quad \text{and} \quad S_2(u, v) = \exp \left[\frac{ik(u^2 + v^2)}{2z} \right]. \quad (5)$$

The main idea now is to improve the approximation of r within the exponentials by incorporating additional terms of the binomial approximation. For this, we recall the binomial series

$$(1 + b)^{1/2} = \sum_{K=0}^{\infty} \binom{1/2}{K} \cdot b^K = 1 + \frac{1}{2}b - \frac{1}{8}b^2 + \frac{1}{16}b^3 - \dots \quad (6)$$

Before we insert r , we have to bring it into a convenient form and reformulate

$$r = [(x - u)^2 + (y - v)^2 + z^2]^{1/2} = z \cdot (1 + b)^{1/2}, \quad (7)$$

with

$$b = \frac{r_{xy}^2}{z^2} + \frac{r_{uv}^2}{z^2} - \frac{2xu}{z^2} - \frac{2yv}{z^2}, \quad (8)$$

and $r_{xy}^2 = x^2 + y^2$ as well as $r_{uv}^2 = u^2 + v^2$. With this prerequisite, we apply Eq. (6) with $n = 1/2$ to Eq. (7) and yield

$$r = z \cdot \sum_{K=0}^{\infty} \binom{1/2}{K} \cdot b^K = z + \frac{r_{xy}^2}{2z} + \frac{r_{uv}^2}{2z} - \frac{xu}{z} - \frac{yv}{z} + z \cdot \sum_{K=2}^{\infty} \binom{1/2}{K} \cdot b^K. \quad (9)$$

In the last step of Eq. (9), we explicitly wrote down the first two summands, corresponding to $K = 0$ and $K = 1$. Please note that they are identical to the approximation of Eq. (3). We can now further separate the higher summands for $K > 1$ into terms that purely depend on either the coordinates of the reconstruction plane, x and y , or on the coordinates of the hologram plane, u and v , and yield

$$\begin{aligned} r = z + \frac{r_{xy}^2}{2z} + \frac{r_{uv}^2}{2z} - \frac{xu}{z} - \frac{yv}{z} + z \cdot \sum_{K=2}^{\infty} \binom{1/2}{K} \left(\frac{r_{xy}^2}{z^2} \right)^K \\ + z \cdot \sum_{K=2}^{\infty} \binom{1/2}{K} \left(\frac{r_{uv}^2}{z^2} \right)^K + z \cdot \sum_{K=2}^{\infty} \mathcal{M}(K). \end{aligned} \quad (10)$$

The last sum contains all of the mixed terms $\mathcal{M}(K)$, which are cross-terms of x, y and u, v . Looking at the definition of the binomial series, we realize that we can rewrite Eq. (10) as

$$r = -z + \sqrt{r_{xy}^2 + z^2} + \sqrt{r_{uv}^2 + z^2} - \frac{xu}{z} - \frac{yv}{z} + z \cdot \sum_{K=2}^{\infty} \mathcal{M}(K). \quad (11)$$

An important requirement of the Fresnel propagation Eq. (4) is the separability of the hologram plane under the integral and the reconstruction plane outside the integral. The only exception are the first order cross-terms $x \cdot u$ and $y \cdot v$, which provide the Fourier transform. Hence, to still ensure separability of the hologram and reconstruction planes, we cannot consider any higher order cross-terms and finally arrive at the approximation

$$r \approx -z + \sqrt{r_{xy}^2 + z^2} + \sqrt{r_{uv}^2 + z^2} - \frac{xu}{z} - \frac{yv}{z}. \quad (12)$$

With this approximation, we preserve the structure of the Fresnel propagation equation [Eq. (4)] and just have to adapt the parabolic phase functions to

$$S_1(x, y) = \exp[ik\sqrt{r_{xy}^2 + z^2} - ikz] \quad \text{and} \quad S_2(u, v) = \exp[ik\sqrt{r_{uv}^2 + z^2}]. \quad (13)$$

If the Fresnel propagation is used to reconstruct the digital holograms, the propagation operator in Eq. (4) has to be inverted, and we find

$$U_O(u, v) = i\lambda z \cdot S_2^*(u, v) \cdot \mathcal{F}^{-1}\{U_H(x, y) \cdot S_1^*(x, y)\} \left(\frac{u}{\lambda z}, \frac{v}{\lambda z} \right), \quad (14)$$

where positive values of z now have the meaning of a reconstruction distance. The approximation in Eq. (14) yields similar reconstruction results to the standard Fresnel approximation. However, in contrast to the Fresnel approximation, the error varies with the radius of the object. This can be seen from the structure of Eq. (11). The mixed terms $\mathcal{M}(K)$ vanish completely on the optical axis, i.e., $x = y = 0$ or $u = v = 0$. Hence, in this case, Eq. (14) is not even an approximation but the exact solution. Consequently, the approximation for surface points close to the optical axis is very good and gets worse with increasing the radius of the object.

2.2 Combining Multiple Reconstructions

We can leverage the relationship between the reconstruction quality and distance from the optical axis by combining reconstructions with the optical axis shifted to different lateral positions. Our improved approximation is exact at $x = y = 0$ as seen when comparing Eqs. (11) and (12). Introducing lateral offsets δx and δy to the optical axis, we reformulate the parabolic phase function accordingly:

$$S_1(x, y) = \exp[ik\sqrt{(x - \delta x)^2 + (y - \delta y)^2 + z^2} - ikz]. \quad (15)$$

This adjustment is still exact along the shifted optical axis at $x = \delta x$ and $y = \delta y$. The shift introduces an additional linear phase term to the reconstruction with tilts $\theta_x = \arctan(\delta x/z)$ and $\theta_y = \arctan(\delta y/z)$. This linear phase can, however, be easily compensated. By stitching the areas of exact reconstruction from multiple propagations with different shifted optical axes, we can combine them to achieve exact reconstructions across large regions of the object plane.

3 Experimental Setup and Results

In the experimental section, we present both simulated results and experimental results to validate the effectiveness of our improved Fresnel propagation method. Both the simulations and the experimental results demonstrate the enhanced quality of hologram reconstruction compared with the standard Fresnel propagation.

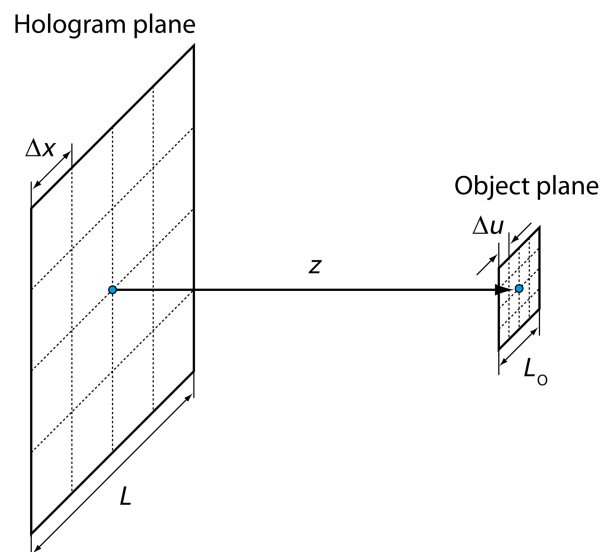


Fig. 1 Typical sampling scheme in lensless microscopy. The hologram plane and the object plane are separated by a distance z . The pixel pitch Δx in the hologram plane is larger than the pitch (resolution) Δu in the object plane. The number of pixels N is invariant, and the Fresnel propagation transforms the pixel pitch in accordance with the diffraction limit.

3.1 Simulative Results

For the initial simulations, we employed a holographic scheme with a plane reference wave and a Siemens star serving as the object. The simulation parameters include the number of pixels $N = 512$, a wavelength of $\lambda = 532$ nm, and a numerical aperture of $NA = 0.26$. The simulated setup is shown schematically in Fig. 1, where we set the pixel pitch in the sensor plane to $\Delta x = 10$ μm and $\Delta u = 1$ μm in the object plane. Rearranging the scaling in Eq. (1), this demands a propagation distance of $z = \Delta x L / \lambda = 9.6$ mm.

To generate an exact hologram, the wave field representing a Siemens star in the object plane was propagated into the sensor plane by solving the Rayleigh–Sommerfeld diffraction formula exactly via direct integration. Afterward, the hologram was reconstructed through Fresnel propagation. Figures 2(a) and 2(b) display the reconstructed amplitude using the standard Fresnel propagation and our improved method, respectively. In addition, Fig. 2(c) shows the reconstructed phase using the standard Fresnel propagation, and Fig. 2(d) shows the reconstructed phase using our method. Notably, our method exhibits superior resolution, finer details in the amplitude, and fewer ripples and distortions in the phase.

As demonstrated in Sec. 2.1 according to Eq. (11), our improved reconstruction method is exact in the center. Thus, we expect a significantly superior result in the reconstruction of a Siemens star, which has its highest spatial frequencies in the center when comparing with the

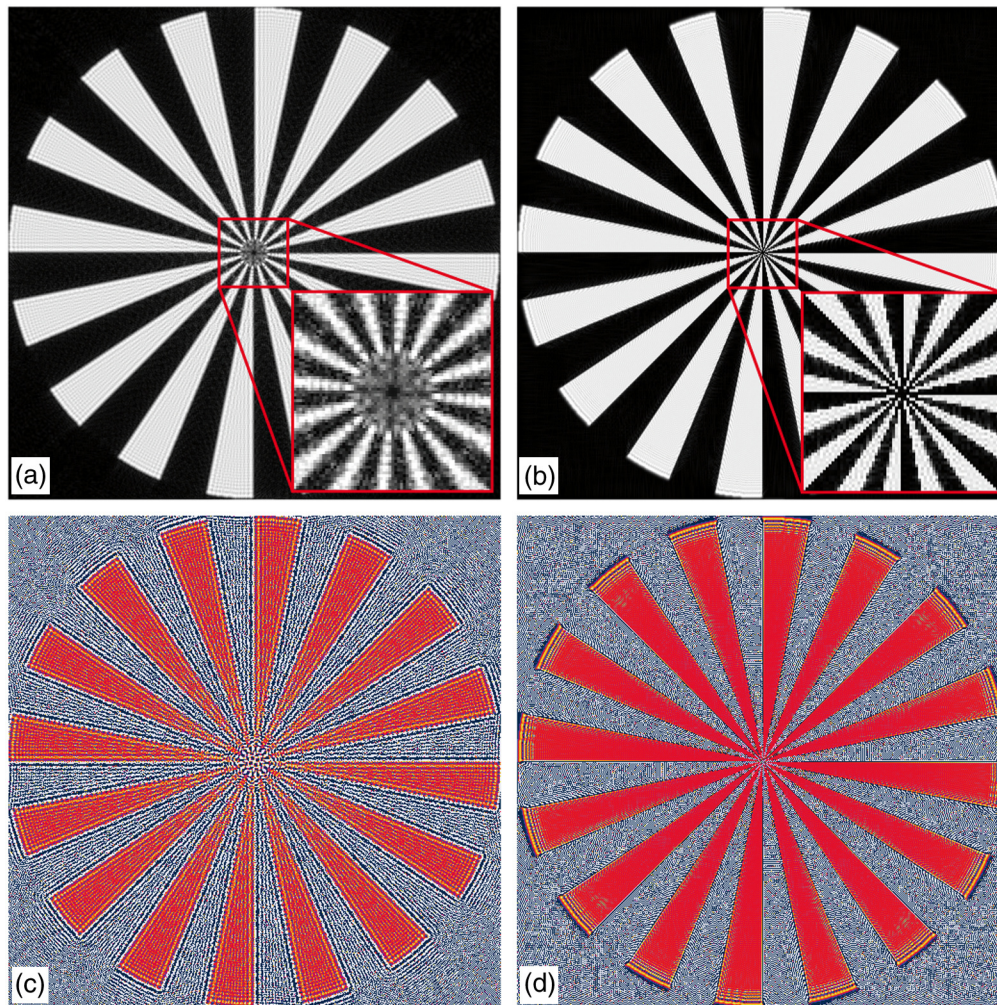


Fig. 2 Reconstructed amplitude and phase of a simulated Siemens star using (a, c) standard Fresnel propagation and (b, d) our improved method. The standard Fresnel reconstruction shows clear degradation of the resolution in the center as well as phase-distortions, whereas our improved reconstruction fully resolves the Siemens star and shows a flat phase distribution except for degradation in the periphery.

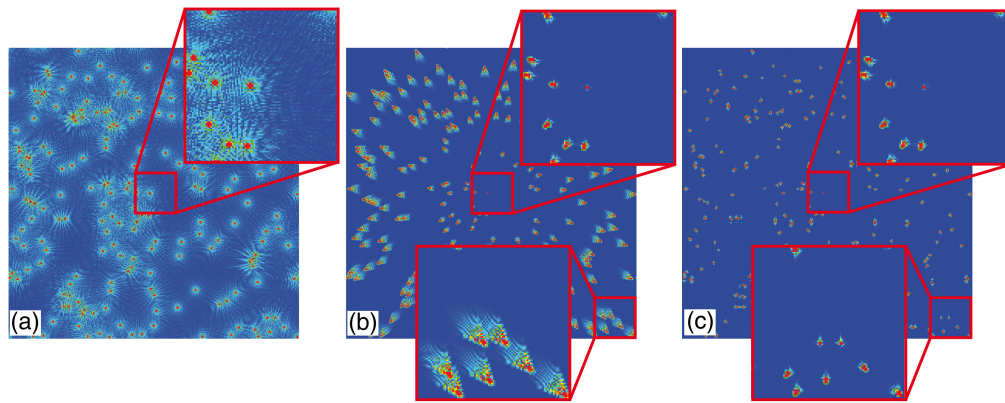


Fig. 3 Amplitude of holographic reconstruction of a randomized dot distribution using (a) standard Fresnel propagation, (b) our improved method, and (c) a combination of 5×5 reconstruction using our improved method with laterally shifted optical axes. The improved Fresnel propagation in (b) shows superior resolution in the center when compared with the standard Fresnel propagation in (a), whereas in the periphery the dots are less well defined. However, the combined reconstruction with shifted optical axes in (c) shows a similarly high resolution in the periphery as in the center.

standard Fresnel propagation. To explore the reconstruction quality in areas far from the optical axis, we used a different object containing a randomized distribution of dots across the object plane. The simulation parameters were exactly the same as with the Siemens star. Figure 3(a) shows the reconstruction of the randomized dot distribution using standard Fresnel propagation; for Fig. 3(b), our improved method was used. When comparing the center region our improved method again exhibits superior resolution, better defined points, and a less disturbed background. However, in the periphery, the size of the reconstructed dots is similar to that of the standard Fresnel propagation.

To achieve a more precise reconstruction across the whole field of view (FoV), we combined multiple holographic reconstructions with a laterally shifted optical axis. We shifted the optical axis laterally to 5×5 different locations across the FoV, each separated by $102.4 \mu\text{m}$. After compensating for the additional phase tilt, the central, exact parts of the individual reconstructions were combined into the overall reconstruction shown in Fig. 3(c). Here, we see in the center that the reconstruction is identical to the improved Fresnel propagation without the optical axis shift. However, due to the combination of multiple exact reconstructions in different areas, the overall reconstruction exhibits a superior resolution of the dots across the whole FoV.

For a quantitative comparison between the reconstruction quality of standard Fresnel propagation and our improved method, we calculated the structural similarity index measure (SSIM) of reconstructions of the “cameraman” test image across varying numerical apertures NA. The SSIM describes the perceived quality of digital images compared to a reference image; an SSIM of 1 indicates perfect similarity, and 0 indicates no similarity.³⁸ A typical reconstruction of the “cameraman” image using 5×5 improved reconstructions with $\text{NA} = 0.3$ is shown in Fig. 4(a) alongside an SSIM map in Fig. 4(b), where dark areas indicate large differences from the original reference image.

Table 1 shows that our improved method outperforms the standard Fresnel reconstruction for every numerical aperture. Furthermore, the reconstruction quality can be improved further by combining multiple reconstructions, especially for larger numerical apertures, i.e., in microscopy scenarios. It should be noted that the computational effort of our improved method is identical to that of standard Fresnel propagation, and every additional reconstruction adds one additional 2D Fourier transformation.

3.2 Experimental Results

The Fresnel propagation alters both the pixel pitch and the FoV of the reconstruction. It is crucial that the illumination remains within the FoV to ensure proper sampling by the camera and to prevent aliasing of the Fresnel reconstruction. Because the FoV in microscopy is typically smaller than the camera target, using plane wave illumination restricted to the FoV would

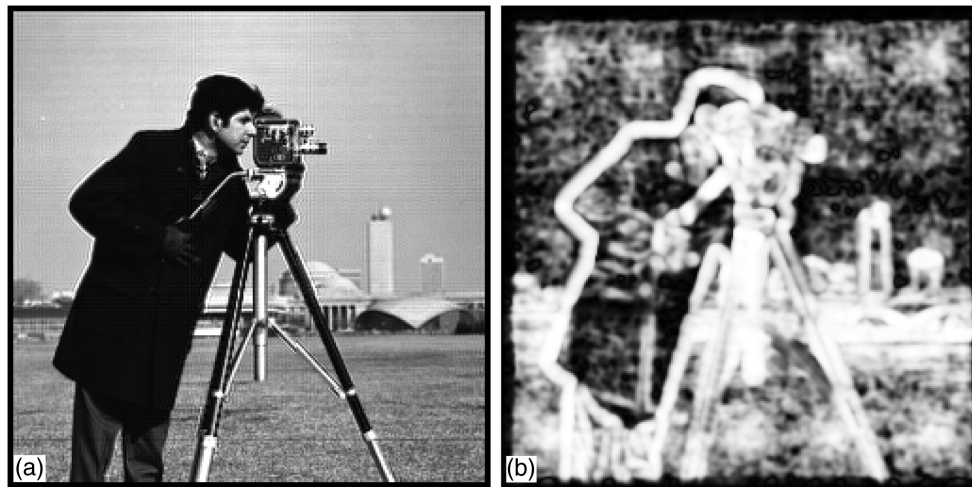


Fig. 4 (a) Amplitude of the reconstruction of the “cameraman” test image with a numerical aperture of $NA = 0.3$, combining 5×5 reconstructions. (b) SSIM map of the reconstruction, where dark areas indicate large differences between the reconstruction and the original reference image.

Table 1 SSIM of reconstructions of the “cameraman” test image reconstructed with varying numerical apertures using standard Fresnel propagation and our improved method using one, 5×5 , and 9×9 reconstructions.

Numerical Aperture	SSIM for			
	Standard Fresnel	Improved Fresnel	Improved Fresnel 5×5	Improved Fresnel 9×9
0.1	0.70	0.78	0.81	0.82
0.3	0.31	0.39	0.55	0.64
0.5	0.20	0.26	0.34	0.41

concentrate most of the recorded light onto a small area of the camera target. To address this issue and improve the signal-to-noise ratio, we utilize divergent illumination, as illustrated in the schematic representation of the setup in Fig. 5(a). The reference wave is shifted laterally to enable off-axis holography.

Divergent illumination can be achieved using point sources, such as monomode fibers. However, conventional monomode fibers offer a numerical aperture of only around 0.1 to 0.2, limiting the illumination of the entire target. To address this, we employ microscope objectives for divergent illumination, as illustrated schematically in Fig. 5(b). It is important to clarify that “lensless imaging” in this context denotes the absence of lenses between the object and camera. The microscope objectives are solely for beam shaping, and they could alternatively be easily substituted, e.g., with tapered fibers featuring higher numerical apertures due to smaller fiber core diameters.

The experimental setup utilized a helium-neon laser with a wavelength of $\lambda = 632.8$ nm as the light source. Imaging was conducted with a camera featuring dimensions of 5120×5120 pixels and a pixel pitch of $2.5 \mu\text{m}$. However, the effective sensor length was constrained to $L = 12.5$ mm by the beam splitter. In Fig. 6(a), the measured digital hologram is shown. Using off-axis holography, the hologram is modulated with high-frequency carrier fringes shown in the inset, which are used for spatial phase shifting in Fourier space [shown in Fig. 6(b)] to reconstruct the complex phase.

The object under investigation is a USAF MIL-STD 150A resolution chart placed in different distances $z = \{120, 29, 16\}$ mm from the camera sensor. With a refractive index of the beam

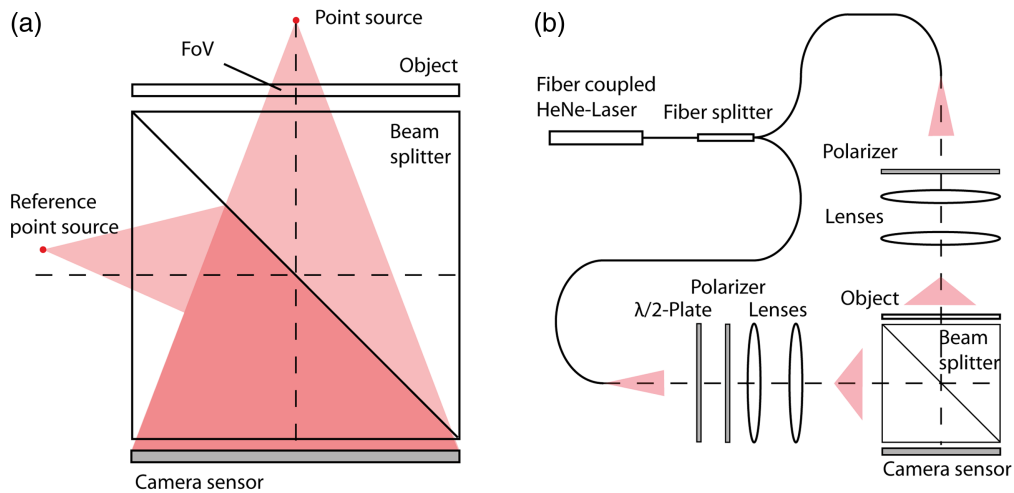


Fig. 5 (a) Detailed schematic illustration of a proposed lensless holographic setup using diverging point light sources for the object illumination and the reference wave, superpositioned on the camera sensor with a beam splitter. The lateral offset of the reference point source enables off-axis holography. (b) Schematic overview of the experimental realization of the holographic setup. A fiber coupled HeNe laser combined with a fused fiber splitter is used to generate the object illumination and reference wave. We employ multiple lenses in both the object and reference path for beam shaping to facilitate high-numerical aperture point source illumination. In addition, the use of polarizers and a $\lambda/2$ -retarder plate ensures maximum contrast of the hologram.

splitter of $n = 1.5$, these configurations yielded a numerical aperture of $NA = \{0.06, 0.26, 0.55\}$, respectively. Consequently, utilizing Fresnel propagation, this results in a pixel pitch $\Delta u = \{5.8, 1.2, 0.5\} \mu\text{m}$ corresponding approximately to the diffraction limit $\delta = \{5.0, 1.0, 0.4\} \mu\text{m}$ in the object plane. Prior to the measurements, the setup was calibrated using a reference measurement conducted across an area of the USAF chart without any surface structure, ensuring accurate measurements.

Figures 7(a)–7(f) show the reconstructions of the recorded holograms for the varying numerical apertures using the standard Fresnel approximation (a, c, e) as well as our improved method (b, d, f). To compare the reconstruction quality between different scenarios, we chose a similar area of the image for each reconstruction. As expected, the reconstructions for both methods are virtually identical for small numerical apertures, as shown in Figs. 7(a) and 7(b), with

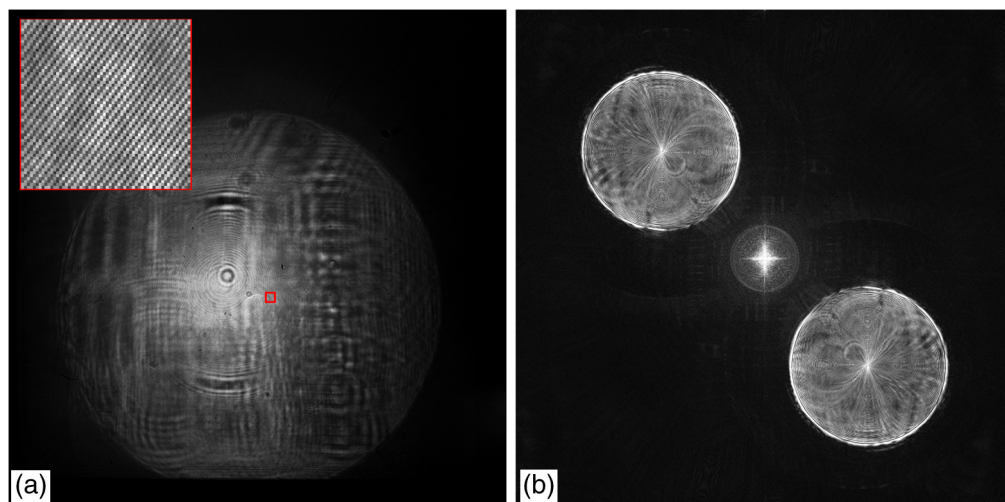


Fig. 6 (a) Digital hologram captured by the camera sensor. Due to the off-axis configuration, the hologram is modulated with carrier fringes as seen in the inset, which shows the small area denoted by the red square. (b) Fourier transformation of the hologram, where the signal can be easily separated from the dc-term for spatial phase shifting.

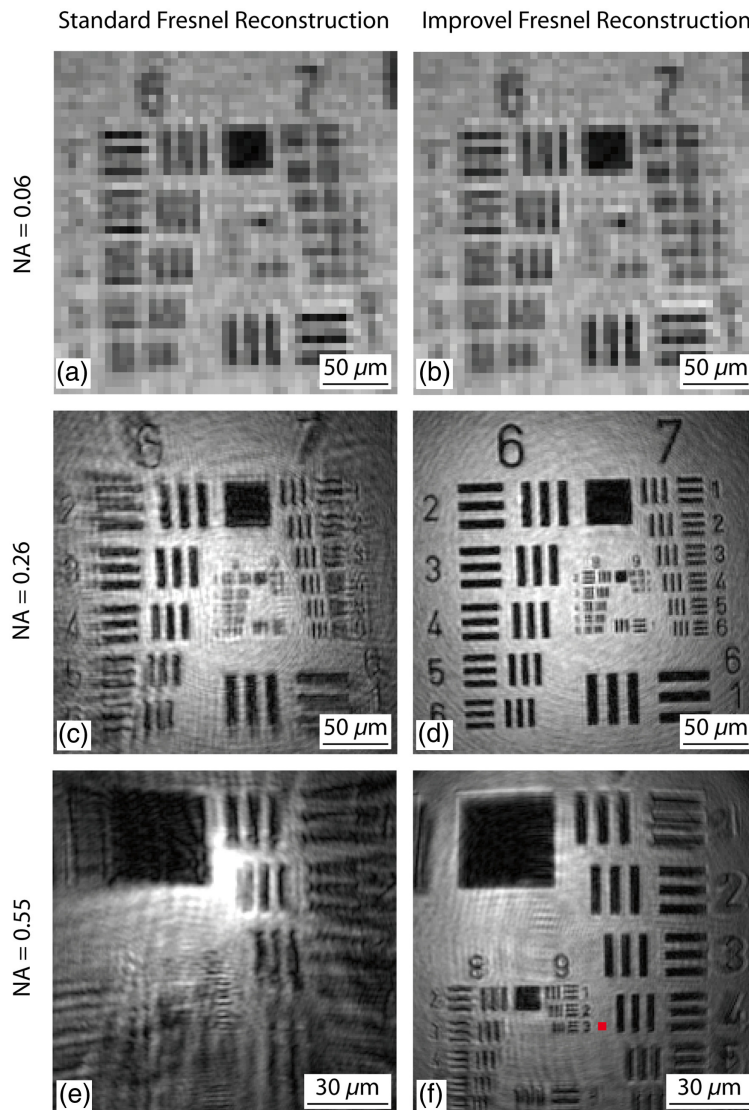


Fig. 7 Holographic reconstructions of a USAF MIL-STD 150A resolution chart using (a, c, e) standard Fresnel propagation and (b, d, f) our improved method for different numerical apertures (a, b) $NA = 0.06$, (c, d) $NA = 0.26$, and (e, f) $NA = 0.55$. For $NA = 0.06$ (a, b) both reconstructions are diffraction limited, (c, e) and the standard Fresnel reconstruction increasingly deteriorates for larger numerical apertures. Our improved reconstructions remain approximately diffraction limited, where for $NA = 0.55$ (f) the smallest available group 9, element 3 with a line width of 780 nm is fully resolved. For reference, the red square indicates the size of a $2.5 \mu\text{m}$ camera pixel.

both reconstruction resolutions being limited by the reconstruction pixel pitch corresponding to the diffraction limit. However, the improved reconstruction remains approximately diffraction limited for higher numerical apertures, whereas the standard Fresnel reconstruction increasingly deteriorates and becomes dominated by imaging errors for high numerical apertures.

Using our improved method at a numerical aperture of $NA = 0.55$, in Fig. 7(f), we can clearly resolve the smallest available element of group 9, which indicates an optical resolution of below $0.8 \mu\text{m}$. For reference, the red square in Fig. 7 indicates the size of a $2.5 \mu\text{m}$ camera pixel and consequently the potential resolution using alternative propagation methods, such as the angular spectrum method.

4 Conclusion

We have presented a novel approach to enhance Fresnel propagation in digital holography, overcoming limitations associated with the traditional Fresnel approximation. By incorporating

higher orders of the binomial approximation, our method extends the applicability of Fresnel propagation to scenarios with larger numerical apertures, thereby significantly improving the reconstruction accuracy. This advancement holds particular significance for lensless holographic microscopy. Because the resolution using a single hologram is generally believed to be limited by the sensor pixel pitch, usually complex scanning schemes are employed to achieve sub-micron resolution. Leveraging the inherent sampling grid transformation of the Fresnel propagation, our improved method achieved sub-micron resolution from a single-shot measurement, allowing for more flexibility and adaptability of lensless microscopy toward transient processes.

Experimental validation demonstrates the effectiveness of our improved Fresnel propagation method, showcasing its superior reconstruction quality compared with standard Fresnel propagation. The simulations and experimental results highlight finer details, improved resolution, and reduced artifacts in both amplitude and phase reconstructions. Notably, with a resolution of below $0.8\ \mu\text{m}$ our method enables the achievement of resolutions significantly below the camera pixel pitch of $2.5\ \mu\text{m}$. Our method does not require any additional computational effort compared with standard Fresnel propagation and can be easily implemented into already existing propagation algorithms and routines, enhancing the accessibility and usability across various fields of research and applications. Furthermore, to locally improve reconstructions, multiple locally exact reconstructions can be combined across the whole FoV.

Disclosures

The authors declare no conflicts of interest.

Code and Data Availability

The data and code presented in this study are available upon reasonable request from the corresponding author.

Acknowledgments

We gratefully acknowledge the Deutsche Forschungsgemeinschaft DFG for funding the research within the project HyperCOMet (Grant No. 430572965). We also thank Bennet Wucherpfennig for support with the experimental measurements.

References

1. D. Gabor, "A new microscopic principle," *Nature* **161**, 777–778 (1948).
2. U. Schnars et al., *Digital Holography and Wavefront Sensing*, 2nd ed., Springer-Verlag, Berlin Heidelberg (2015).
3. C. Falldorf et al., "Flash-profilometry: fullfield lensless acquisition of spectral holograms for coherence scanning profilometry," *Opt. Express* **31**(17), 27494–27507 (2023).
4. P. J. de Groot et al., "Contributions of holography to the advancement of interferometric measurements of surface topography," *Light: Adv. Manuf.* **3**(2), 258–277 (2022).
5. M. Fratz et al., "Digital holography in production: an overview," *Light: Adv. Manuf.* **2**(3), 283–295 (2021).
6. C. Falldorf, M. Agour, and R. B. Bergmann, "Digital holography and quantitative phase contrast imaging using computational shear interferometry," *Opt. Eng.* **54**(2), 024110 (2015).
7. V. Balasubramani et al., "Holographic tomography: techniques and biomedical applications," *Appl. Opt.* **60**(10), B65–B80 (2021).
8. M. Agour et al., "Quantitative phase contrast imaging of microinjection molded parts using computational shear interferometry," *IEEE Trans. Ind. Inf.* **12**(4), 1623–1630 (2015).
9. J. An et al., "Slim-panel holographic video display," *Nat. Commun.* **11**(1), 5568 (2020).
10. D. E. Smalley et al., "Anisotropic leaky-mode modulator for holographic video displays," *Nature* **498**(7454), 313–317 (2013).
11. C. Falldorf et al., "Functional pixels: a pathway towards true holographic displays using today's display technology," *Opt. Express* **30**(26), 47528–47540 (2022).
12. A. F. Müller et al., "Multicolor holographic display of 3D scenes using referenceless phase holography (RELPH)," *Photonics* **8**(7), 247 (2021).

13. G. Pedrini and H. J. Tiziani, "Short-coherence digital microscopy by use of a lensless holographic imaging system," *Appl. Opt.* **41**(22), 4489–4496 (2002).
14. A. Ozcan and E. McLeod, "Lensless imaging and sensing," *Annu. Rev. Biomed. Eng.* **18**, 77–102 (2016).
15. V. Boominathan et al., "Recent advances in lensless imaging," *Optica* **9**(1), 1–16 (2022).
16. H. Tobon-Maya et al., "Open-source, cost-effective, portable, 3D-printed digital lensless holographic microscope," *Appl. Opt.* **60**(4), A205–A214 (2021).
17. M. Lee, O. Yaglidere, and A. Ozcan, "Field-portable reflection and transmission microscopy based on lensless holography," *Biomed. Opt. Express* **2**(9), 2721–2730 (2011).
18. D. Chen et al., "Resolution and contrast enhancement for lensless digital holographic microscopy and its application in biomedicine," *Photonics* **9**(5), 358 (2022).
19. Y. Wu and A. Ozcan, "Lensless digital holographic microscopy and its applications in biomedicine and environmental monitoring," *Methods* **136**, 4–16 (2018).
20. T. Shimobaba, T. Kakue, and T. Ito, "Review of fast algorithms and hardware implementations on computer holography," *IEEE Trans. Ind. Inf.* **12**(4), 1611–1622 (2015).
21. J.-C. Li et al., "Digital holographic reconstruction of large objects using a convolution approach and adjustable magnification," *Opt. Lett.* **34**(5), 572–574 (2009).
22. J. F. Restrepo and J. Garcia-Sucerquia, "Magnified reconstruction of digitally recorded holograms by Fresnel–Bluestein transform," *Appl. Opt.* **49**(33), 6430–6435 (2010).
23. P. Gao and C. Yuan, "Resolution enhancement of digital holographic microscopy via synthetic aperture: a review," *Light: Adv. Manuf.* **3**(1), 105–120 (2022).
24. V. Micó, C. Ferreira, and J. García, "Surpassing digital holography limits by lensless object scanning holography," *Opt. Express* **20**(9), 9382–9395 (2012).
25. J. H. Massig, "Digital off-axis holography with a synthetic aperture," *Opt. Lett.* **27**(24), 2179–2181 (2002).
26. A. Greenbaum et al., "Wide-field computational imaging of pathology slides using lens-free on-chip microscopy," *Sci. Transl. Med.* **6**(267), 267ra175 (2014).
27. J. Di et al., "High resolution digital holographic microscopy with a wide field of view based on a synthetic aperture technique and use of linear CCD scanning," *Appl. Opt.* **47**(30), 5654–5659 (2008).
28. V. Bianco, M. Paturzo, and P. Ferraro, "Spatio-temporal scanning modality for synthesizing interferograms and digital holograms," *Opt. Express* **22**(19), 22328–22339 (2014).
29. W. Bishara, H. Zhu, and A. Ozcan, "Holographic opto-fluidic microscopy," *Opt. Express* **18**(26), 27499–27510 (2010).
30. T.-W. Su et al., "Multi-angle lensless digital holography for depth resolved imaging on a chip," *Opt. Express* **18**(9), 9690–9711 (2010).
31. W. Bishara et al., "Holographic pixel super-resolution in portable lensless on-chip microscopy using a fiber-optic array," *Lab Chip* **11**(7), 1276–1279 (2011).
32. M. Paturzo et al., "Super-resolution in digital holography by a two-dimensional dynamic phase grating," *Opt. Express* **16**(21), 17107–17118 (2008).
33. C. Liu et al., "Super-resolution digital holographic imaging method," *Appl. Phys. Lett.* **81**(17), 3143–3145 (2002).
34. R. Grella, "Fresnel propagation and diffraction and paraxial wave equation," *J. Opt.* **13**(6), 367 (1982).
35. D. Wang et al., "High-fidelity numerical realization of multiple-step Fresnel propagation for the reconstruction of digital holograms," *Appl. Opt.* **47**, D12–D20 (2008).
36. J. W. Goodman, *Introduction to Fourier Optics*, Roberts and Company Publishers (2005).
37. V. Nascov and P. C. Logofătu, "Fast computation algorithm for the rayleigh-sommerfeld diffraction formula using a type of scaled convolution," *Appl. Opt.* **48**(22), 4310–4319 (2009).
38. Z. Wang et al., "Image quality assessment: from error visibility to structural similarity," *IEEE Trans. Image Process.* **13**(4), 600–612 (2004).

André F. Müller has studied physics at the University of Bremen, Germany. He is currently a research scientist at Bremer Institut für angewandte Strahltechnik (BIAS), Germany. His main research interests are in optical metrology and digital holography, particularly lensless digital holographic microscopy as well as the analysis of partially coherent wave fields applied to aspheric and freeform testing, for which he won the young scientist award of the German association of applied optics in 2020.

Ralf B. Bergmann studied physics, received his doctorate from the University of Stuttgart for his work at the Max Planck Institute for Solid State Research, joined the University of New South Wales as a postdoc and habilitated at the University of Freiburg. He headed a research group at the University of Stuttgart and a research department at Robert Bosch Cooperate Research. In 2008, he became a professor at the University of Bremen and head of BIAS.

Claas Falldorf received his PhD in physics and has over 20 years of expertise in coherent optics. He is the head of the Coherent Optics and Nanophotonics Group at the BIAS. He authored more than 150 publications in areas, such as optical metrology, light field synthesis, and digital holography and is the co-author of the book *Digital Holography and Wavefront Sensing*, which is considered a standard work for digital holography.